



PERGAMON

Computers & Fluids 32 (2003) 223–248

**computers
&
fluids**

www.elsevier.com/locate/complfluid

Element residual error estimate for the finite volume method

H. Jasak ^{a,*}, A.D. Gosman ^b

^a *Nabla Ltd., The Mews, Picketts Lodge, Picketts Lane, Salfords, Surrey RH1 5RG, UK*

^b *Department of Mechanical Engineering, Imperial College of Science, Technology and Medicine, London SW7 2BX, UK*

Received 3 January 2000; received in revised form 25 September 2001; accepted 1 October 2001

Abstract

Out of the wide range of *a-posteriori* error estimates for the finite element method (FEM), the group of estimates based on the element residual seems to be the most popular. One recent extension of the element residual method is the element residual error estimate (EREE) [Numerische Mathematik 65 (1993) 23], which includes the elements of the duality theory and consistently produces good results. In this paper, the EREE will be extended to allow its use in conjunction with the finite volume (FV) type of discretisation. The extension consists of three parts: an appropriate definition of the residual in the FV framework, a procedure for calculation of self-equilibrating fluxes based on the conservative properties of the FV solution and a simplified solution method for the Local Problem. The paper covers the extensions of the EREE to the convection–diffusion and the Navier–Stokes problem, following [Comp Meth Appl Mech Engng 101 (1992) 73] and [Comp Meth Appl Mech Engng 111 (1994) 185], respectively. The error estimate is tested on three test cases with analytical solutions, where its performance is shown to be similar to its FEM counterpart. Finally, the estimate is applied to a realistic laminar fluid flow problem.

© 2002 Elsevier Science Ltd. All rights reserved.

Keywords: Error estimation; Finite volume; Element residual method

1. Introduction

The finite element method (FEM) of discretisation offers a wide range of popular *a-posteriori* error estimates. Oden et al. [4] present five groups of error estimators: the element- and sub-domain-residual methods, duality methods, interpolation and post-processing methods. Element

* Corresponding author. Tel.: +44-020-7221-9815.

E-mail addresses: h.jasak@nabla.co.uk (H. Jasak), d.gosman@ic.ac.uk (A.D. Gosman).

residual methods use the residual in the numerical solution to estimate the local error, where the residual is a function measuring how much the approximate solution fails to satisfy the governing differential equation and boundary conditions for the particular finite element. Duality methods use the duality theory of convex optimisation to derive the upper and lower bounds of the error for self-adjoint problems. Sub-domain-residual methods are based on the solution of the local error problem over a patch of finite elements. Interpolation methods use the FEM interpolation theory to produce a crude estimate of the leading term of the truncation error. Post-processing methods are based on the fact that the solution (which is expected to be smooth) can be improved by an appropriate smoothing algorithm. The error estimate is obtained by comparing the post-processed version of the solution with the one obtained from the actual calculation. All these methods are strongly mathematically based and their properties have been examined for a wide range of shape functions, not only for symmetric boundary value problems but also for convection–diffusion problems. A comprehensive review of Finite Element error analysis can be found in [5].

The element residual error estimate (EREE) is a relative newcomer in the error estimation for FEM. It has been developed mainly by Ainsworth and Oden [1,2,6] and Ainsworth [7], but also includes the previous work by Bank [8], Bank and Weiser [8,9] and Kelly [10].¹ The method has also been extended to the Navier–Stokes problem in the work of Oden et al. [3,11]. It consistently gives highly accurate estimates for a large variety of problems. This error estimate gives a strict upper bound on the solution error in the energy norm. It requires the solution of a local error problem over each finite element and an error flux equilibration procedure. The error flux equilibration has been discussed at length by Kelly [10] and Ainsworth and Oden [6]. Kelly shows that non-equilibrated fluxes result in a gross over-estimation of the solution error. The analysis of the flux equilibration problem has also been given by Ainsworth and Oden [1,5]. Recent work of Oden et al. [11] presents an adaptive refinement technique based on this error estimate applied to the incompressible Navier–Stokes equations.

In comparison with the abundance of FEM error estimates, the finite volume (FV) error estimation is still in early stages of development. The only widely-used a-posteriori error estimate is Richardson extrapolation [12–15], which in turn requires two solutions on meshes with different spacing. Apart from several attempts aimed at measuring the numerical diffusion [16,17], the scope of single-mesh single-run error estimates aimed at the complete discretisation error is very limited. Some interesting attempts include the cell imbalance error estimate by Haworth et al. [18], the method based on higher order face interpolation by Muzaferija [19] and the Taylor series and moment error estimate by Jasak [20,21], respectively based on the Taylor series truncation error analysis and the imbalance in the higher moments of the solution.

In order to extend the EREE to the FV discretisation successfully, it is first necessary to formulate the cell residual in a manner equivalent to its meaning in FEM. It will be shown that this residual is a consequence of the inconsistency between the prescribed variation of the solution over the control volume (CV) used for the volume integration and the one used for face inter-

¹ In [5] this error estimate is referred to as the equilibrated residual method, as extension of the EREE which requires error flux equilibration.

polation. An error estimate based directly on the FV version of the residual has been presented in [22] but it lacks the upper bound property of the EREE.

In this paper, the above-mentioned definition of the residual will be used as a basis for the modification of the EREE from the FEM into a form suitable for the finite volume method (FVM). The approach by Ainsworth and Oden [1] has been chosen as the most general and directly extensible to the FV discretisation. The basic error estimate will be developed first for a linear elliptic problem and subsequently extended to convection–diffusion [2] and non-linear problems, specifically incompressible Navier–Stokes equations [3]. In Section 2, the construction of the residual in the FV framework will be examined. The conservation properties of the FVM removes the need for a special error flux balancing algorithm, as will be shown in Section 3.2. A simplified solution procedure for the local error problem is given in Section 4. In Section 5, the new error estimate is examined on several test cases with analytical solutions. Once its performance has been established, the error estimate will be applied to a realistic test case, consisting of a 2-D laminar flow over a hill.

2. Construction of the residual

The definition of a residual in the FEM arises naturally from the discretisation process. The equations are discretised and solved using the variational principle, where the weighted sum of residuals is minimised to produce the solution. The residual is a consequence of the fact that the exact solution can locally change faster than the prescribed (n th order) shape function over the finite element, thus creating a discretisation error.

FV discretisation is based on the integral form of the equation over the CV. CVs do not overlap, and cover the complete computational domain. The FVM guarantees that the equation will be satisfied over each CV in the integral form. On the other hand, the prescription of the local variation of the variable is still necessary which, in FEM terms, should produce a local residual. Our task is to establish why the residual does not occur naturally, and to reconstruct it from the solution. We shall start with a brief overview of the second-order accurate FV discretisation on arbitrarily unstructured meshes [19,21,23–25].

2.1. Overview of the finite volume discretisation

Consider the standard form of the steady-state transport equation for a general tensorial property ϕ :

$$\nabla \cdot (\mathbf{u}\phi) - \nabla \cdot (\gamma \nabla \phi) = S - L\phi, \quad (1)$$

where \mathbf{u} is the velocity field, $\gamma \geq 0$ is the effective diffusivity coefficient and S and $L \geq 0$ represent the linear decomposition of any other (source) terms.

The FVM uses the integral form of Eq. (1) over the CV:

$$\int_{V_p} \nabla \cdot (\mathbf{u}\phi) dV - \int_{V_p} \nabla \cdot (\gamma \nabla \phi) dV = \int_{V_p} (S - L\phi) dV. \quad (2)$$

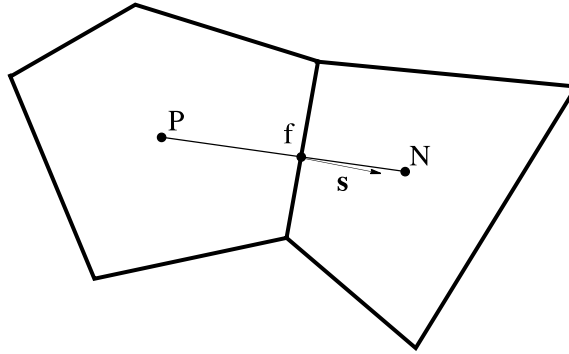


Fig. 1. Control volume.

The geometry of a CV, Fig. 1, is described by the location of its centroid P where ϕ is calculated, its volume V_P and the flat faces f bounding it. The face f , described by the associated face area vector \mathbf{s} , is shared with one neighbouring CV (N). The vector $\mathbf{d} \equiv \overline{PN}$, connecting the two cell centres around the face is also defined. It is required for every face that $\mathbf{d} \cdot \mathbf{s} > 0$. We shall also introduce a unit normal to the face f :

$$\hat{\mathbf{n}}_f = \frac{\mathbf{s}_f}{|\mathbf{s}_f|}. \quad (3)$$

Internal faces of the mesh are ordered in such a way that $\hat{\mathbf{n}}_f$ points into the cell appearing later in the cell list.

The divergence terms in Eq. (2) can be transformed into surface integrals using the Gauss' theorem. A second-order accurate approximation of the integrals in Eq. (2) is obtained by prescribing a linear variation of ϕ over the CV:

$$\phi(\mathbf{x}) = \phi_P + (\mathbf{x} - \mathbf{x}_P) \cdot (\nabla\phi)_P, \quad (4)$$

where $\phi_P = \phi(\mathbf{x}_P)$ and $(\nabla\phi)_P = \nabla\phi(\mathbf{x}_P)$. The integrals are now calculated using the mid-point rule, leading to the following semi-discretised version of Eq. (2):

$$\sum_f F\phi_f - \sum_f \gamma_f \mathbf{s} \cdot (\nabla\phi)_f = SV_P - L\phi_P V_P, \quad (5)$$

where F is the convective face flux:

$$F = \mathbf{u}_f \cdot \mathbf{s}, \quad (6)$$

which satisfies the continuity constraint (if any).

The discretisation is completed when the face values ϕ_f and $(\nabla\phi)_f$ are expressed in terms of the cell centre values ϕ_P and ϕ_N around the face (Fig. 1). In the simplest form, we can assume:

$$\phi_f = f_x \phi_P + (1 - f_x) \phi_N \quad (7)$$

$$f_x = \frac{\overrightarrow{Pf} \cdot \mathbf{s}}{\mathbf{d} \cdot \mathbf{s}}, \quad (8)$$

where f_x is the interpolation factor and

$$\mathbf{s} \cdot (\nabla \phi)_f = |\mathbf{s}| \frac{\phi_N - \phi_P}{|\mathbf{d}|}, \tag{9}$$

with an appropriate “non-orthogonal correction” if $\mathbf{d} \nparallel \mathbf{s}$ [21]. The result of discretisation is a linear equation (one for each CV):

$$a_P \phi_P + \sum_N a_N \phi_N = R_P. \tag{10}$$

The value of ϕ_P depends on the values in the neighbouring cells, thus creating a system of algebraic equations:

$$[A][\phi] = [R], \tag{11}$$

where $[A]$ is a sparse matrix, with coefficients a_P on the diagonal and a_N off the diagonal; $[\phi]$ is the vector of ϕ -s for all CVs and $[R]$ is the right-hand side vector.

2.2. Formulation of the residual

The inter-point coupling in the system of algebraic equations obtained by the FVM comes from the face interpolation. The cell value of ϕ depends on the values in neighbouring cells through the face values and gradients of ϕ , Eqs. (7) and (9). Inconsistency between the volume integration and face interpolation can be explained on a simple 1-D situation (Fig. 2).

When the volume integral is calculated, it is assumed that the variation of ϕ over the CV is linear, Eq. (4). At the same time, face interpolation in Eqs. (7) and (9) assumes that ϕ varies linearly between P and N (Fig. 2). For an arbitrary point A inside the CV, two equally valid values of ϕ can be given: one consistent with the volume integration and another consistent with the face interpolation. The two values will be the same only if the discretisation error is equal to zero.

The FVM guarantees that Eq. (2) will be satisfied only with the combination of the cell and face integrals described above. The cell residual is therefore hidden in the inconsistency between the two “shape functions”. It can be recreated by strictly adhering to one of the functions described above, in our case Eq. (4):

$$\phi_f = \phi_P + (\mathbf{x}_f - \mathbf{x}_P) \cdot \nabla \phi_P \tag{12}$$

and

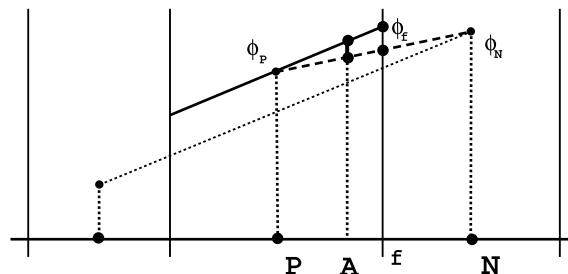


Fig. 2. Face interpolation and cell volume integration.

$$(\nabla\phi)_f = \nabla\phi_P. \quad (13)$$

The cell residual for Eq. (2), assembled as:

$$\begin{aligned} r_P &= \int_{V_P} [S - L\phi_P - \nabla \cdot (\mathbf{u}\phi) + \nabla \cdot (\gamma\nabla\phi)] dV \\ &= SV_P - L\phi_P V_P - \sum_f [F\phi_f - \gamma_f \mathbf{s} \cdot (\nabla\phi)_f] \end{aligned} \quad (14)$$

will be non-zero even when Eq. (11) is solved to machine tolerance. This formulation is consistent with the FEM meaning of the residual, measuring how well the prescribed shape function approximates the solution over the cell.

3. Element residual error estimate

The EREE [1] in the FEM extends and combines several existing error estimation techniques to the non-uniform h - p FE approximation² on irregular meshes, and derives a strict upper bound on the solution error expressed through an error norm. The error estimate requires a solution of a local residual problem over every cell after the residual is assembled, as described in the previous Section.

In what follows, the error estimate is first developed for an elliptic model problem in Section 3.1. Section 3.2 presents the error flux balancing in the FVM context; this issue and the consequences of non-equilibrated error fluxes have been discussed in detail in has been discussed in [5]. It will be shown that, unlike in the FEM, the equilibrated error fluxes are readily available from the FV solution. Generalisation to the scalar transport equation and the Navier–Stokes problem is given in Sections 3.3 and 3.4, respectively. A simplified solution procedure for the local problem in the FVM framework is given in Section 4.

For the details of the derivation of the EREE, the reader is referred to [1]. This Section will only present the basic principles and their extension to the FV discretisation without mathematical proof.

3.1. Elliptic model problem

The model problem that is being solved is:

$$-\nabla \cdot (\gamma\nabla\phi) = S - L\phi \quad \text{in } \Omega, \quad (15)$$

with the diffusion constant $\gamma > 0$, the volume source constants S and L and the following boundary conditions:

$$\begin{cases} \phi = 0 & \text{on } \Gamma_D, \\ \gamma\hat{\mathbf{n}}_f \cdot \nabla\phi = g & \text{on } \Gamma_N, \end{cases} \quad (16)$$

² Here, h -refinement implies a change in the mesh size, whereas p -refinement modifies the local order of discretisation.

with

$$\begin{aligned} \Gamma_D \cap \Gamma_N &= \emptyset, \\ \Gamma_D \cup \Gamma_N &= \partial\Omega. \end{aligned} \tag{17}$$

Let us now introduce a new way of presenting the error which has been accepted as standard in FEM applications—an error norm.

The error norm $\|e\|_E^2$ for the elliptic problem, Eq. (15), is defined as:

$$\|e\|_E^2 = \int_V (\gamma \nabla e \cdot \nabla e + Le^2) dV, \tag{18}$$

where e is the error, defined as the difference between the exact (ϕ) and numerical (ϕ_h) solution:

$$e = \phi - \phi_h. \tag{19}$$

This norm is the “energy norm”.

An important property of this norm is the scaling [1]:

$$\|e\|_E = \|\phi - \phi_h\| \leq Ch^k, \tag{20}$$

where h is the linear size (e.g. diameter) of the CV, k is the order of approximation and C is a constant independent of h and k . The error norm scales correctly on a non-uniform h - p mesh, which is important in the case of local refinement.

Through a series of theorems, Ainsworth and Oden [1] derive the following property:

Theorem 1. *For every sub-domain, a local problem:*

$$-\nabla \cdot \nabla \psi = r_p \quad \text{in } \Omega_p, \tag{21}$$

with boundary conditions:

$$\begin{cases} \hat{\mathbf{n}}_f \cdot \nabla \psi = j & \text{on } \partial\Omega_p \setminus \Gamma_D, \\ \psi = 0 & \text{on } \partial\Omega_p \cap \Gamma_D, \end{cases} \tag{22}$$

can be used to produce a local error estimate:

$$\epsilon_p^2(\nabla \psi) = \int_{\Omega_p} \frac{1}{\gamma} \nabla \psi \cdot \nabla \psi dV. \tag{23}$$

This error estimate provides the strict global upper bound on the exact error in the energy norm:

$$\|e\|_E^2 \leq \sum_{P=1}^N \epsilon_P^2(\nabla \psi), \tag{24}$$

where

- Ω_p is the local sub-domain, usually a single CV,
- r_p is the solution residual over Ω_p :

$$r_p = \int_{\Omega_p} r dV = \int_{\Omega_p} [S - L\phi_h + \nabla \cdot (\gamma \nabla \phi_h)] dV, \tag{25}$$

- j is the residual error flux defined below,
- N is the number of sub-domains.

It is worth pointing out that the boundary value problem, Eq. (21), has a solution only under specific circumstances, depending on the combination of r_P and the boundary conditions, Eq. (22). This is usually termed the “flux equilibration problem” and will be revisited in Section 3.2.

As can be seen from the form of Eq. (21), local problems are coupled through the boundary conditions, specifically through the residual error flux j , dependent on the face jumps in the solution. The calculation of the error fluxes in FEM has been discussed in detail in a number of papers [1,7].

Following [1], j is defined as:

$$j = \begin{cases} g - \gamma \hat{\mathbf{n}}_f \cdot \nabla \phi_h & \text{on } \partial\Omega_P \cap \Gamma_N, \\ -\alpha \llbracket \gamma \hat{\mathbf{n}}_f \cdot \nabla \phi_h \rrbracket & \text{on } \partial\Omega_P \setminus \Gamma_N. \end{cases} \quad (26)$$

The term $\llbracket \gamma \hat{\mathbf{n}}_f \cdot \nabla \phi_h \rrbracket$ is defined on each internal face of the mesh as the local jump in the gradient:

$$\llbracket \gamma \hat{\mathbf{n}}_f \cdot \nabla \phi_h \rrbracket = \left[\gamma \hat{\mathbf{n}}_f \cdot (\nabla \phi_h)_f \right]_P - \left[\gamma \hat{\mathbf{n}}_f \cdot (\nabla \phi_h)_f \right]_N, \quad (27)$$

where P and N are the CVs sharing the face. Similarly, the face jump is:

$$\llbracket \phi_h \rrbracket = [(\phi_h)_f]_P - [(\phi_h)_f]_N. \quad (28)$$

Here, $[(\phi_h)_f]_P$ and $[(\nabla \phi_h)_f]_P$ are the values of ϕ_h and $\nabla \phi_h$ on the face f consistent with the prescribed variation of ϕ_h in the cell P .

We can also define an arbitrary linear interpolate of $(\phi_h)_f$ and $(\gamma \hat{\mathbf{n}}_f \cdot \nabla \phi_h)_f$:

$$\langle \gamma \hat{\mathbf{n}}_f \cdot \nabla \phi_h \rangle_\alpha = \alpha \gamma \hat{\mathbf{n}}_f \cdot [(\nabla \phi_h)_f]_P + (1 - \alpha) \gamma \hat{\mathbf{n}}_f \cdot [(\nabla \phi_h)_f]_N \quad (29)$$

$$\langle \phi_h \rangle_\alpha = \alpha [(\phi_h)_f]_P + (1 - \alpha) [(\phi_h)_f]_N. \quad (30)$$

Nothing needs to be said about α in Eqs. (29) and (30) apart from that it is the same as in Eq. (26).

3.2. Balancing problem in the finite volume method

The necessary condition for the solution of the local problem is that the error fluxes are balanced [1]:

$$\int_{\Omega_P} r \, dV + \oint_{\partial\Omega_P} j \, dA = 0. \quad (31)$$

The problem of determining α in such a way that Eq. (31) is satisfied is crucial, as the performance of the error estimate is critically dependent on this condition. If the error fluxes are not balanced, the accuracy of the error estimate is degraded to such an extent that the error bound of Eq. (24) becomes meaningless [1,5].

The balancing procedure determines the boundary conditions for local error problems, Eq. (22), in such a way that Eq. (31) is satisfied for every CV. The balanced error fluxes can be computed without the need to calculate the α -s, based on the conservation properties of the FVM. Error flux balancing will be done here for the elliptic problem, Eq. (15), and subsequently

generalised to the convection–diffusion and the Navier–Stokes problems. In order to simplify the expressions, the subscript h will be dropped. Face values of ϕ and $\nabla\phi$ are assumed when they are needed (i.e. on all mesh faces).

Separating the boundary conditions, the residual can be written as:

$$\int_{\Omega_P} r \, dV = \underbrace{\int_{\Omega_P} (S - L\phi_P) \, dV}_a + \underbrace{\int_{\partial\Omega_P \setminus \Gamma_D} \gamma \, ds \cdot \nabla\phi_P}_b. \tag{32}$$

The integral of the face jump can be split into two parts using Eq. (26):

$$\int_{\partial\Omega_P} j \, dA = \underbrace{\int_{\partial\Omega_P \cap \Gamma_N} (g - \gamma \hat{\mathbf{n}}_f \cdot \nabla\phi_P) \, dA}_c + \underbrace{\int_{\partial\Omega_P \setminus \Gamma_N} -\alpha [\gamma \hat{\mathbf{n}}_f \cdot \nabla\phi]}_d \, dA. \tag{33}$$

The term (b) from Eq. (32) can also be split into two, depending on the boundary condition:

$$\int_{\partial\Omega_P \setminus \Gamma_D} \gamma \, ds \cdot \nabla\phi_P = \underbrace{\int_{\partial\Omega_P \cap \Gamma_N} \gamma \, ds \cdot \nabla\phi_P}_e + \underbrace{\int_{\partial\Omega_P \setminus \Gamma_N \setminus \Gamma_D} \gamma \, ds \cdot \nabla\phi_P}_f. \tag{34}$$

The residual balance condition, Eq. (31), will now be assembled part by part, using Eqs. (32)–(34). To clarify further developments, the reader is reminded that j is not defined on Γ_D , as this is not necessary (see boundary conditions for the local problem, Eq. (22)).

Combining Eq. (33) (c) and Eq. (34) (e) yields:

$$\int_{\partial\Omega_P \cap \Gamma_N} (g - \gamma \hat{\mathbf{n}}_f \cdot \nabla\phi_P) \, dA + \int_{\partial\Omega_P \cap \Gamma_N} \gamma \, ds \cdot \nabla\phi_P = \int_{\partial\Omega_P \cap \Gamma_N} g \, dA. \tag{35}$$

Combining Eq. (33) (d) and Eq. (34) (f) yields:

$$\begin{aligned} & \int_{\partial\Omega_P \setminus \Gamma_N} -\alpha [\gamma \hat{\mathbf{n}}_f \cdot \nabla\phi] \, dA + \int_{\partial\Omega_P \setminus \Gamma_N \setminus \Gamma_D} \gamma \, ds \cdot \nabla\phi_P \\ &= \int_{\partial\Omega_P \setminus \Gamma_N \setminus \Gamma_D} [\gamma \hat{\mathbf{n}}_f \cdot \nabla\phi_P - \alpha(\gamma \hat{\mathbf{n}}_f \cdot \nabla\phi_P - \gamma \hat{\mathbf{n}}_f \cdot \nabla\phi_N)] \, dA \\ &= \int_{\partial\Omega_P \setminus \Gamma_N \setminus \Gamma_D} [(1 - \alpha)\gamma \hat{\mathbf{n}}_f \cdot \nabla\phi_P + \alpha\gamma \hat{\mathbf{n}}_f \cdot \nabla\phi_N] \, dA \\ &= \int_{\partial\Omega_P \setminus \Gamma_N \setminus \Gamma_D} \langle \gamma \hat{\mathbf{n}}_f \cdot \nabla\phi \rangle_{(1-\alpha)} \, dA, \end{aligned} \tag{36}$$

where (see Eq. (29)):

$$\langle \gamma \hat{\mathbf{n}}_f \cdot \nabla\phi \rangle_{(1-\alpha)} = (1 - \alpha)\gamma \hat{\mathbf{n}}_f \cdot \nabla\phi_P + \alpha\gamma \hat{\mathbf{n}}_f \cdot \nabla\phi_N. \tag{37}$$

Assembling the balance, Eq. (31), from Eqs. (32), (35) and (36), it follows:

$$\int_{\Omega_P} (S - L\phi_P) \, dV + \int_{\partial\Omega_P \cap \Gamma_N} g \, dA + \int_{\partial\Omega_P \setminus \Gamma_N \setminus \Gamma_D} \langle \gamma \hat{\mathbf{n}}_f \cdot \nabla\phi \rangle_{(1-\alpha)} \, dA = 0. \tag{38}$$

The result can be interpreted as follows: the interpolation method for the face fluxes $\langle \gamma \hat{\mathbf{n}}_f \cdot \nabla \phi \rangle_{(1-\alpha)}$ is such that, together with the volume integral, they satisfy the original problem, Eq. (15), in the integral form over each CV.

Eq. (38) provides a basis for the calculation of balanced fluxes. In the first stage, the calculation of j can be modified. On internal faces of the mesh, j is:

$$\begin{aligned} -\alpha \llbracket \gamma \hat{\mathbf{n}}_f \cdot \nabla \phi \rrbracket &= -\alpha (\gamma \hat{\mathbf{n}}_f \cdot \nabla \phi_P - \gamma \hat{\mathbf{n}}_f \cdot \nabla \phi_N) \\ &= (1 - \alpha) \gamma \hat{\mathbf{n}}_f \cdot \nabla \phi_P + \alpha \gamma \hat{\mathbf{n}}_f \cdot \nabla \phi_N - \gamma \hat{\mathbf{n}}_f \cdot \nabla \phi_P \\ &= \langle \gamma \hat{\mathbf{n}}_f \cdot \nabla \phi \rangle_{(1-\alpha)} - \gamma \hat{\mathbf{n}}_f \cdot \nabla \phi_P. \end{aligned} \quad (39)$$

On boundary faces, Eq. (26) can be used directly.

It remains to determine the interpolate $\langle \gamma \hat{\mathbf{n}}_f \cdot \nabla \phi \rangle_{(1-\alpha)}$. Fortunately, the FVM readily provides these fluxes. As a consequence of the conservative property of the discretisation, the face fluxes calculated consistently with the discretisation automatically satisfy Eq. (38)

For the model problem, the interpolated face gradient is

$$\langle \gamma \hat{\mathbf{n}}_f \cdot \nabla \phi \rangle_{(1-\alpha)} = \gamma \frac{\phi_N - \phi_P}{|\mathbf{d}|}. \quad (40)$$

The balance condition, Eq. (38), is satisfied to the solver tolerance. The calculation of j is straightforward (Eq. (39)) and it does not require the explicit evaluation of α for the faces.

3.3. Convection–diffusion problem

In order to apply the EREE to the convection–diffusion problem, we need to incorporate the convection term into the analysis presented above. This generalisation is based on its FEM equivalent presented in [2]. The contribution of the convection term to the residual has been presented in Section 2. The balanced error flux uses the interpolated value of ϕ_h to the face. For completeness, the expressions for the residual and j are given below.

A steady-state convection–diffusion problem is specified as follows: Find $\phi = \phi(\mathbf{x})$ such that

$$\nabla \cdot (\mathbf{u}\phi) - \nabla \cdot (\gamma \nabla \phi) = S - L\phi \quad \text{in } \Omega, \quad (41)$$

with boundary conditions:

$$\begin{cases} \phi = \phi_D(\mathbf{x}) & \text{on } \Gamma_D, \\ \gamma \hat{\mathbf{n}}_f \cdot \nabla \phi = g(\mathbf{x}) & \text{on } \Gamma_N, \end{cases} \quad (42)$$

where

$$\Gamma_D \cap \Gamma_N = \emptyset,$$

$$\Gamma_D \cup \Gamma_N = \partial\Omega$$

and $L \geq 0$, $\gamma > 0$. The residual for a given numerical solution $\phi_h(\mathbf{x})$ is:

$$r_P = \int_{\Omega_P} r \, dV = \int_{\Omega_P} [S - L\phi_h - \nabla \cdot (\mathbf{u}\phi_h) + \nabla \cdot (\gamma \nabla \phi_h)] \, dV, \quad (43)$$

or, introducing $\phi_P = \phi_h(\mathbf{x}_P)$ and $\phi_f = \phi_f(\mathbf{x}_f)$:

$$r_P = SV_P - L\phi_P V_P - \sum_f \mathbf{s} \cdot [(\mathbf{u})_f \phi_f - \gamma(\nabla\phi_h)_f], \tag{44}$$

consistent with Eq. (14). The residual error fluxes which satisfy the balance condition are:

- On internal faces:

$$j = \alpha u_f [\phi_h] - \alpha [\gamma \hat{\mathbf{n}}_f \cdot \nabla \phi_h] = u_f (-\langle \phi_h \rangle_{(1-\alpha)} + \phi_f) - (-\langle \gamma \hat{\mathbf{n}}_f \cdot \nabla \phi_h \rangle_{(1-\alpha)} + \gamma \hat{\mathbf{n}}_f \cdot (\nabla \phi_h)_f), \tag{45}$$

- On fixed gradient boundary faces (Γ_N):

$$j = \alpha u_f [\phi_h] - \alpha [\gamma \hat{\mathbf{n}}_f \cdot \nabla \phi_h] = u_f (-\langle \phi_h \rangle_{(1-\alpha)} + \phi_f) - (-g + \gamma \hat{\mathbf{n}}_f \cdot (\nabla \phi_h)_f), \tag{46}$$

- On fixed value boundary faces, the calculation of j splits into two parts:

1. For the convection part, the face jump exists:

$$j_C = \alpha u_f [\phi_h] = u_f (-\langle \phi_h \rangle_{(1-\alpha)} + \phi_f). \tag{47}$$

2. For the diffusion part, Γ_D is treated as a fixed value boundary from the elliptic problem. Since the exact boundary gradient is not known, the local problem has to be solved with the fixed value boundary condition. This somewhat complicates matters, as the residual also contains the face jump from the convection term, Eq. (47). An appropriate modification is, however, easily introduced. Before the solution of the local problem, the part of the residual from the convection term on the fixed value boundary will be removed; thereafter the boundary can be treated in the same way as before.

In Eqs. (45)–(47) u_f is the face velocity defined with respect to the direction of the face area vector.

$$u_f = \hat{\mathbf{n}}_f \cdot \mathbf{u}_f, \tag{48}$$

where $\hat{\mathbf{n}}_f$ is the face normal. Note that in practice either $u_f = F/|s|$ or $u_f = -F/|s|$, depending on the ordering of cells and faces. $\langle \phi_h \rangle_{(1-\alpha)}$ in Eqs. (45)–(47) is calculated consistently with the convection differencing scheme (in our case Eqs. (7) and (8)). The error norm for the convection–diffusion problem has the following form [2]:

$$\|e\|_E^2 = \|\phi - \phi_h\|_E^2 = \int_V (\gamma \nabla e \cdot \nabla e + L e^2) dV. \tag{49}$$

The local problem is:

$$-\nabla \cdot \nabla \psi = r_P \quad \text{in } \Omega_P, \tag{50}$$

with boundary conditions:

$$\begin{cases} \hat{\mathbf{n}}_f \cdot \nabla \psi = j & \text{on } \partial\Omega_P \setminus \Gamma_D, \\ \hat{\mathbf{n}}_f \cdot \nabla \psi = j_C, \psi = 0 & \text{on } \partial\Omega_P \cap \Gamma_D. \end{cases} \tag{51}$$

The upper bound for the error in the convection–diffusion problem is the same as for the elliptic case:

$$\|e\|_E^2 \leq \sum_{P=1}^N \epsilon_P^2 (\nabla \psi), \tag{52}$$

where

$$\epsilon_p^2(\nabla\psi) = \int_{\Omega_p} \left(\frac{1}{\gamma} \nabla\psi \cdot \nabla\psi \right) dV. \quad (53)$$

This concludes the extension of the EREE to the convection–diffusion problem.

3.4. Navier–Stokes problem

The form of the EREE for the Navier–Stokes equations is similar to the one for the scalar transport equation and it follows the derivation presented in [3]. Some points, however, need to be discussed further: the formulation of an appropriate error norm for the Navier–Stokes problem and the coupling between the pressure error and the convection–diffusion error.

Let us first formulate the incompressible steady laminar form of the Navier–Stokes problem: Find the pair $(\mathbf{u}(\mathbf{x}), p(\mathbf{x}))$ such that

$$\begin{cases} \nabla \cdot (\mathbf{u}\mathbf{u} - \nu\nabla\mathbf{u}) = \mathbf{f} - \nabla p, \\ \nabla \cdot \mathbf{u} = 0 \end{cases} \quad (54)$$

in Ω , with the boundary conditions:

$$\begin{cases} \mathbf{u} = \mathbf{u}_D(\mathbf{x}), & \nabla p = 0 & \text{on } \Gamma_D, \\ \hat{\mathbf{n}}_f \cdot \nabla\mathbf{u} = 0, & p = p_N(\mathbf{x}) & \text{on } \Gamma_N, \end{cases} \quad (55)$$

where:

$$\Gamma_D \cap \Gamma_N = \emptyset,$$

$$\Gamma_D \cup \Gamma_N = \partial\Omega$$

and $\nu > 0$.

3.4.1. Error norm for the Navier–Stokes system

In order to simplify the discussion, from here on all the variables will be considered to be dimensionless, with the characteristic scales equal to unity (following [26]). If the uniqueness condition [3,26,27] for the solution is satisfied, the following property of the numerical solution can be proven (see [3,26]):

Theorem 2. *Suppose that the conditions for the uniqueness of the solution for the Navier–Stokes problem hold. Let (\mathbf{u}, p) be the solution of Eq. (54). Then, for ν sufficiently large, there exists a mesh spacing h_0 such that for all $h \leq h_0$, the discretised form of Eq. (54) has a unique solution (\mathbf{u}_h, p_h) and*

$$\lim_{h \rightarrow 0} (|\mathbf{u} - \mathbf{u}_h|_1 + \|p - p_h\|_0) = 0. \quad (56)$$

If, in addition, the solution (\mathbf{u}, p) of Eq. (54) is in the space of accessible functions of order $k + 1$, where k is the order of accuracy of the discretisation method, then a constant $C > 0$ exists, independent of k , such that

$$|\mathbf{u} - \mathbf{u}_h|_1 + \|p - p_h\|_0 \leq Ch^k. \quad (57)$$

The norms used above are:

$$\|\mathbf{v}\|_1^2 = \int_{\Omega} v(\nabla\mathbf{v}:\nabla\mathbf{v}) dV, \tag{58}$$

$$\|q\|_0^2 = \int_{\Omega} q^2 dV. \tag{59}$$

The error in the solution for Eq. (54) is defined as:

$$\mathbf{e} = \mathbf{u} - \mathbf{u}_h, \tag{60}$$

$$E = p - p_h. \tag{61}$$

We shall introduce a new “star” norm which bounds the error [3,28]:

$$\|(\mathbf{e}, E)\|_* = \int_{\Omega} v(\nabla\mathbf{e}:\nabla\mathbf{e}) dV + \int_{\Omega} (\nabla \cdot \mathbf{u}_h)^2 dV. \tag{62}$$

3.4.2. Formulation of the local problem

Let \mathbf{m}_p be the solution of the local problem [3]:

$$-\nabla \cdot \nabla\mathbf{m} = \mathbf{r}_p \quad \text{in } \Omega_p, \tag{63}$$

with boundary conditions:

$$\begin{cases} \hat{\mathbf{n}}_f \cdot \nabla\mathbf{m} = \mathbf{j} & \text{on } \partial\Omega_p \setminus \Gamma_D, \\ \hat{\mathbf{n}}_f \cdot \nabla\mathbf{m} = \mathbf{j}_C, \mathbf{m} = \mathbf{0} & \text{on } \partial\Omega_p \cap \Gamma_D. \end{cases} \tag{64}$$

Introducing $\mathbf{u}_p = \mathbf{u}_h(\mathbf{x}_p)$ and $\mathbf{u}_f = \mathbf{u}_h(\mathbf{x}_f)$, the residual \mathbf{r}_p and face jumps \mathbf{j} and \mathbf{j}_C are:

$$\mathbf{r}_p = \int_{\Omega_p} \mathbf{r} dV = \int_{\Omega_p} [\mathbf{f} - \nabla p_h - \nabla \cdot (\mathbf{u}_h \mathbf{u}_h - v \nabla \mathbf{u}_h)] dV, \tag{65}$$

on internal faces:

$$\mathbf{j} = u_f(-\langle \mathbf{u}_h \rangle_{(1-\alpha)} + \mathbf{u}_f) - [-\langle v \hat{\mathbf{n}}_f \cdot \nabla \mathbf{u}_h \rangle_{(1-\alpha)} + v \hat{\mathbf{n}}_f \cdot (\nabla \mathbf{u}_h)_f], \tag{66}$$

on zero gradient boundary faces:

$$\mathbf{j} = u_f(-\langle \mathbf{u}_h \rangle_{(1-\alpha)} + \mathbf{u}_f) - v \hat{\mathbf{n}}_f \cdot (\nabla \mathbf{u}_h)_f \tag{67}$$

and on fixed value boundary faces:

$$\mathbf{j}_C = u_f(-\langle \mathbf{u}_h \rangle_{(1-\alpha)} + \mathbf{u}_f). \tag{68}$$

Then, the error (\mathbf{e}, E) of the discrete solution of the Navier–Stokes problem, Eq. (54), satisfies the following bound:

$$\|(\mathbf{e}, E)\|_*^2 \leq \sum_{P=1}^N \epsilon_P^2 (\nabla\mathbf{m}, \nabla \cdot \mathbf{u}_h), \tag{69}$$

where N is the number of sub-domains.

The local error estimate $\epsilon_p^2(\nabla \mathbf{m}, \nabla \cdot \mathbf{u}_h)$ is defined as:

$$\epsilon_p^2(\nabla \mathbf{m}, \nabla \cdot \mathbf{u}_h) = \int_{\Omega_p} \left(\frac{1}{v} \nabla \mathbf{m} : \nabla \mathbf{m} \right) dV + \int_{\Omega_p} (\nabla \cdot \mathbf{u}_h)^2 dV. \quad (70)$$

The only difference between the convection–diffusion and the Navier–Stokes problem is the treatment of the additional “source” term: the pressure gradient. In the convection–diffusion problem, constant source terms are considered to be exact, whereas here the pressure gradient term carries a certain numerical error of its own, associated with the divergence of velocity.

4. Solution of the local problem

The results on the upper bound for the error, Eqs. (24), (52) and (69), assume that the local problem is solved exactly over each sub-domain. In FEM, this is usually done by extending the set of available shape functions with so-called “bubble-functions”. The solution is, however, potentially expensive and for purposes of error estimation (which carries its own level of uncertainty) not really necessary. It should, however, be noted that without solving the local problem exactly one cannot accept the preserve the upper bound mentioned above. In this Section, we shall examine the nature of the local problem and propose a simple approximate solution method. Numerical experiments show that this method is appropriate our purposes.

Let us first reexamine the definition of the local problem for the elliptic equation, Eqs. (21) and (22):

$$-\nabla \cdot \nabla \psi = r_p \quad \text{in } \Omega_p, \quad (71)$$

with boundary conditions:

$$\begin{cases} \hat{\mathbf{n}}_f \cdot \nabla \psi = j & \text{on } \partial\Omega_p \setminus \Gamma_D, \\ \psi = 0 & \text{on } \partial\Omega_p \cap \Gamma_D. \end{cases} \quad (72)$$

The boundary conditions show a certain peculiarity: the problem is well-posed only if the CV has a face on Γ_D ; otherwise it is indeterminate to a constant. The actual error estimate does not require ψ , but only the volume integral of its gradient.

4.1. Indeterminate local problem

The indeterminate form of Eq. (21) has fixed gradient boundary conditions on all boundaries. Eq. (21) shows that the distribution of ψ through the domain is quadratic, or in other words, $\nabla \psi$ varies linearly. It is therefore only necessary to determine $\nabla \psi$ in the centroid of the domain (in our case a single CV) and use the mid-point rule to calculate the integral. This is done by applying a weighted linear fit to Eq. (22):

$$\nabla \psi = \frac{1}{V_p} \sum_f \mathbf{s} | \mathbf{x}_f - \mathbf{x}_P | \hat{\mathbf{n}}_f \cdot \nabla \psi_f = \frac{1}{V_p} \sum_f \mathbf{s} | \mathbf{x}_f - \mathbf{x}_P | (j)_f. \quad (73)$$

Although it now seems that the error estimate does not depend on the cell residual, as r_P does not feature in Eq. (73), the reader should be reminded that Eq. (31) imposes a strict link between the residual and Eq. (22). The local error estimate is now:

$$\epsilon_P^2(\nabla\psi) = \int_{\Omega_P} \frac{1}{\gamma} \nabla\psi \cdot \nabla\psi \, dV = \frac{1}{\gamma V_P} \left(\sum_f \mathbf{s} |\mathbf{x}_f - \mathbf{x}_P| (j)_f \right)^2 \tag{74}$$

4.2. Determinate local problem

If the local error problem is determinate, the elegance of the above procedure is no longer directly applicable. However, we can produce a cheap estimate of the solution by neglecting the variation of the error flux along the fixed value boundary. The “missing” j is determined from the balance condition, Eq. (31) and the result from the previous Section is used. This is done by formally solving the local problem on a 1-cell mesh.

The local problem is discretised using the Gauss’ theorem:

$$- \sum_f \mathbf{s} \cdot (\nabla\psi)_f = r_P. \tag{75}$$

The faces with the fixed gradient boundary condition will be called the “g”-faces and the faces with the fixed value boundary condition the “v”-faces. The sum from Eq. (75) splits into two:

$$\sum_f \mathbf{s} \cdot (\nabla\psi)_f = \sum_g \mathbf{s} \cdot (\nabla\psi)_g + \sum_v \mathbf{s} \cdot (\nabla\psi)_v. \tag{76}$$

For the “g”-faces, the boundary condition is given:

$$\mathbf{s} \cdot (\nabla\psi)_g = |\mathbf{s}| \hat{\mathbf{n}}_f \cdot (\nabla\psi)_g = |\mathbf{s}| j_g, \tag{77}$$

whereas for the “v”-faces we have:

$$\mathbf{s} \cdot (\nabla\psi)_v = |\mathbf{s}| \hat{\mathbf{n}}_f \cdot (\nabla\psi)_v = |\mathbf{s}| \frac{(\psi)_v - (\psi)_P}{|\mathbf{d}|}. \tag{78}$$

Here, $(\psi)_P$ is the solution of the local problem in the cell centre. $(\psi)_v$ is equal to zero, following the boundary condition on the local problem, Eq. (22).

$(\psi)_P$ is therefore:

$$(\psi)_P = \frac{r_P + \sum_g |\mathbf{s}| j_g}{\sum_v |\mathbf{s}| \frac{1}{|\mathbf{d}|}} \tag{79}$$

and the face gradients for the “v”-faces are

$$\hat{\mathbf{n}}_f \cdot (\nabla\psi)_v = \frac{-(\psi)_P}{|\mathbf{d}|}. \tag{80}$$

All face gradients are now known and Eq. (73) can again be used.

The simplification described above assumes at most a linear variation of the error flux along the fixed value boundary face, thus introducing a certain error. However, an equivalent assumption is made in the discretised boundary condition in the FVM. Consequently, the authors here acknowledge the potential source of inaccuracy and examine its consequences in the next section.

5. Test cases

Three numerical examples will be presented in increasing order of complexity: an elliptic model problem with fixed-value boundary conditions [2] in Section 5.1; a convection–diffusion of a scalar in Section 5.2; and finally in Section 5.3, we shall tackle a fluid flow example. The accuracy of the proposed solution method for the local problem will also be examined. Once the performance of the error estimate has been established, it will be used on a realistic fluid flow case: a laminar flow over a 2-D hill.

5.1. Elliptic model problem

Consider [2]:

$$-\nabla \cdot \nabla \phi = 0 \quad \text{in } \Omega: \left[0, \frac{1}{2}\right] \times \left[0, \frac{1}{2}\right], \quad (81)$$

with boundary conditions:

$$\begin{cases} \phi(0, y) = \left(e^{-\sqrt{1+4\pi^2}} - 1\right) \sin(2\pi y), \\ \phi\left(\frac{1}{2}, y\right) = \phi(x, 0) = \phi\left(x, \frac{1}{2}\right) = 0. \end{cases} \quad (82)$$

The solution of the problem is:

$$\phi(x, y) = e^{(x-1)\sqrt{1+2\pi^2}} - e^{-x\sqrt{1+4\pi^2}} \sin(2\pi y). \quad (83)$$

The exact solution on a 10×10 mesh and the estimated error norm distribution for the numerical solution are shown in Fig. 3(a) and (b), respectively.

The exact and estimated global energy norms for the error are used to calculate the global effectiveness index:

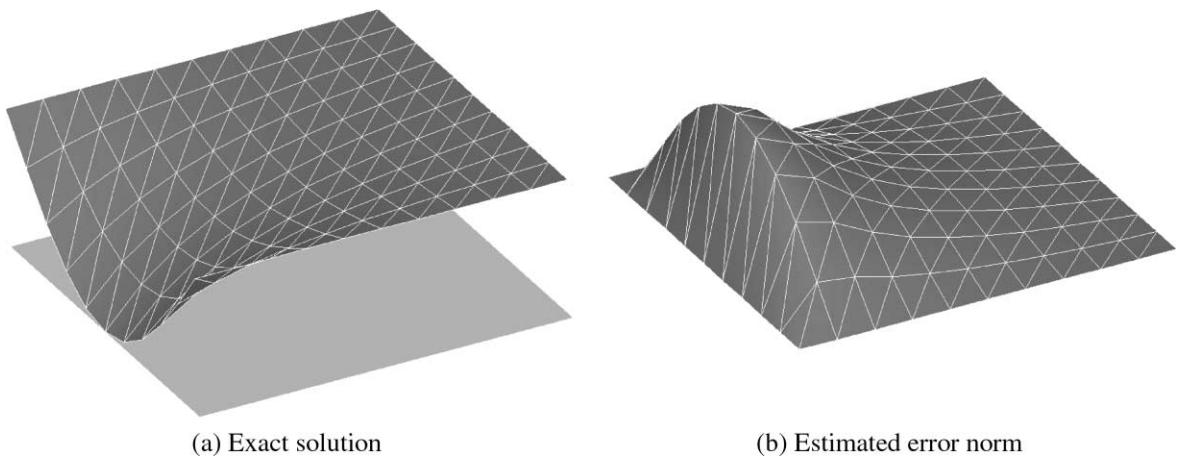


Fig. 3. Elliptic test case.

$$\zeta = \frac{\|e\|_{\text{est}}}{\|e\|_{\text{exact}}} = \frac{0.052461605}{0.0513568} = 1.021. \tag{84}$$

Let us now consider the accuracy of the solution procedure for the local problem presented in Section 4. For that purpose, two CVs are selected: one for the determinate local problem (i.e. with a face on the fixed value boundary) and one for the indeterminate form. The boundary conditions are calculated from the balanced error fluxes, as explained in Section 3. The local problem is solved numerically on a 200×200 CV mesh (over the single CV of the original mesh) and using the simple procedure described above.

For the indeterminate local problem, the difference between the two solutions is less than 0.02%, actually measuring the error in the numerical solution. For the determinate local problem, the inaccuracy of the simplified solution is up to 20%. However, having in mind that: (i) the error estimate only provides the limit on the global error and not the error distribution; (ii) the relative proportion of CVs with a boundary face drops quickly with the mesh size (e.g. 36% on a 10×10 CV mesh and 3.9% on a 100×100 CV mesh in 2-D); (iii) the approximate solution method is cheap and simple, the simplified solution procedure from Section 4 is considered appropriate.

5.2. Line source in cross flow

The second test case is the convective–diffusive transport of a passive scalar in a fixed uniform velocity field. The mesh is aligned with the flow and the boundary conditions are shown in Fig. 4.

The analytical solution can be found in [29]:

$$\phi(x, y) = \frac{S^*}{2\pi\gamma} K_0 \left(\frac{U_1 \sqrt{x^2 + y^2}}{2\gamma} \right) \exp \left(\frac{U_1 x}{2\gamma} \right), \tag{85}$$

where x and y are the spatial coordinates. The origin of the coordinate system is located at the source, with the x coordinate pointing in the direction of the velocity vector, $S^* = 16.67[\phi]/s$ is the strength of the source, $\gamma = 0.05 \text{ m}^2/s$ is the diffusion coefficient, $U_1 = 1 \text{ m/s}$ is magnitude of the velocity and K_0 is the zeroth order modified Bessel function of the second kind.

The exact solution and the distribution of the estimated error norm for the mesh with 40×21 CVs are given in Fig. 5.

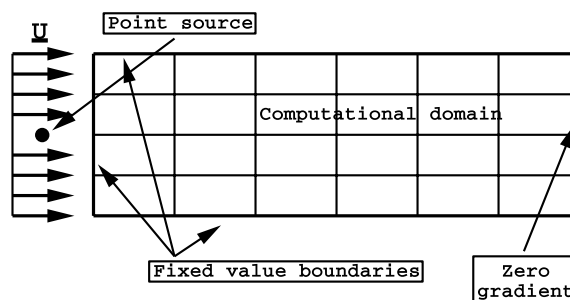


Fig. 4. Line source in cross flow, test setup.

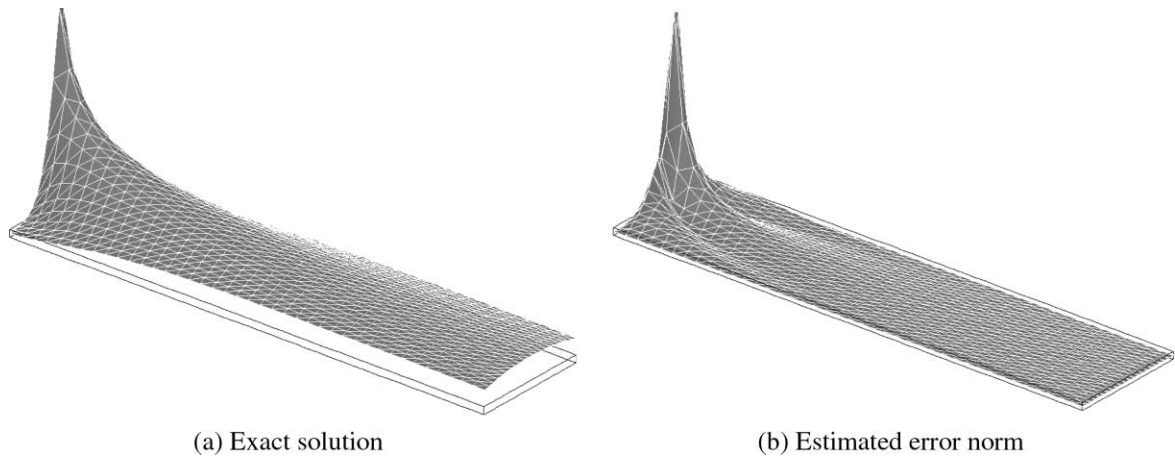


Fig. 5. Line source in cross flow.

Table 1

Line source in cross flow: global error norm and effectiveness index

Mesh size	Global error norm	Global effectiveness index
10×5	4.56203	1.32034
20×11	2.32105	1.10746
40×21	1.219	0.95054

Effectiveness indices on several meshes are given in Table 1.

In uniformly refined meshes, the distribution of the estimated error will always be similar to the one shown in Fig. 5. If, however, error-driven adaptive refinement is used instead, the error distribution will also depend on the local mesh size.

In order to examine the performance of the error estimate on non-uniform meshes, the above test case will be solved using the mesh refinement scheme described in [30]. Mesh refinement is driven by the estimated error distribution and oriented normally to the local solution gradient. A “1-irregularity” criterion [30] is enforced to preserve mesh smoothness.

Two adaptive calculations are performed, starting from a coarse initial mesh (60 CVs) and an intermediate mesh (3200 CVs). A sequence of refined meshes for the first case is shown in Fig. 6.

A corresponding sequence of estimated error norm distribution for the above meshes is presented in Fig. 7. Note that the scale on all plots has been adjusted to account for the decrease in the peak estimated error. The location of the peak error also moves, which is caused by the interaction between the local mesh resolution and the solution gradient.

Fig. 8 shows the scaling of the error estimate with mesh refinement for a series of meshes, ranging from 50 to 51 520 CV. It can be seen that the estimate exhibits the second-order error reduction, consistent with the order of discretisation. It is also evident that error-driven automatic adaptive refinement considerably outperforms systematic uniform refinement for this case.

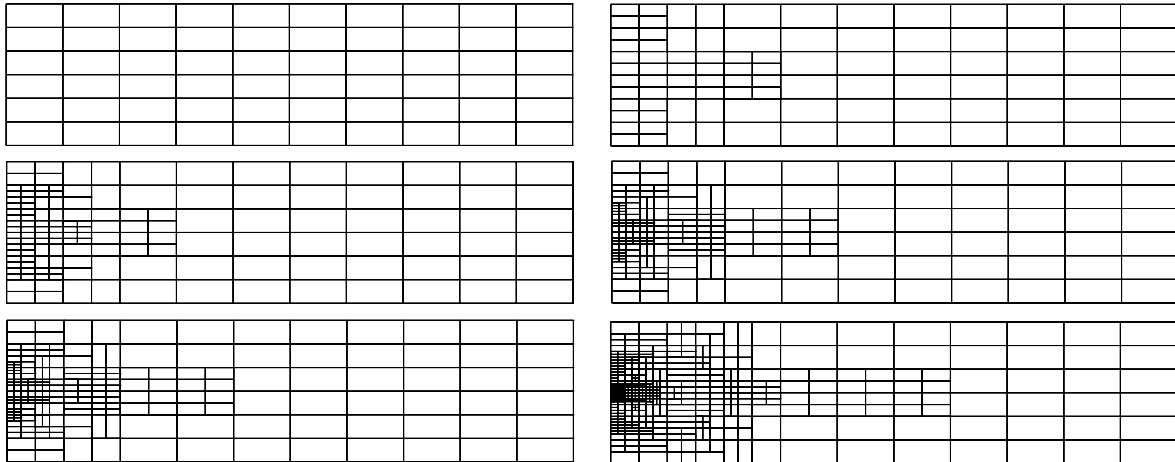


Fig. 6. Line source: error-driven local mesh refinement.

5.3. Line jet

Having considered an elliptic and a convection–diffusion test case, we shall now consider a model laminar Navier–Stokes Problem. It is an infinitely fast jet emanating from an infinitely thin line orifice entering a large domain. The momentum of the jet is finite and equal to M_j . The analytical solution can be found in [31]:

$$\mathbf{u} = u\mathbf{i} + v\mathbf{j}, \tag{86}$$

where

$$u = \frac{A}{B}x^{-1/3} \operatorname{sech}^2\left(x^{-2/3}\frac{y}{B}\right), \tag{87}$$

$$v = -\frac{1}{3}Ax^{-2/3} \tanh\left(x^{-2/3}\frac{y}{B}\right) + \frac{2}{3}\frac{A}{B}x^{-4/3}y \operatorname{sech}^2\left(x^{-2/3}\frac{y}{B}\right), \tag{88}$$

$$A = \left(\frac{9}{2}vM_j\right)^{1/3}, \tag{89}$$

$$B = \left(\frac{48v^2}{M_j}\right)^{1/3} \tag{90}$$

and $M_j = U_0^2h$ is the momentum carried by the jet. The test setup on the 4×1 m in size, 0.5 m downstream of the orifice is shown in Fig. 9. The exact solution and the error norm distribution for the 40×21 CV mesh are shown in Fig. 10. The estimated error correctly highlights the region close to the orifice where the high error is caused by the high velocity gradients. Downstream of the jet, the velocity field is smoother, causing a lower error.

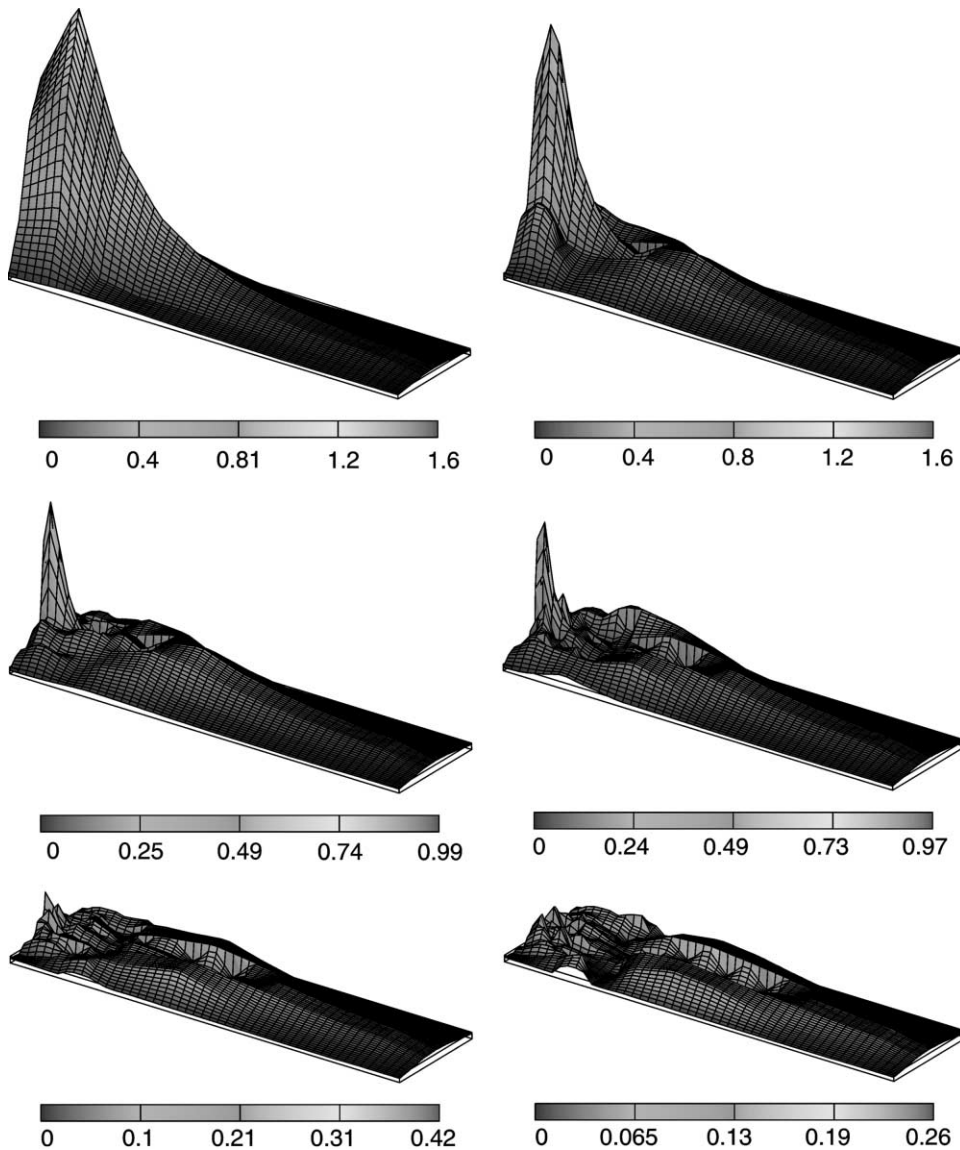


Fig. 7. Line source: error norm distribution for local refinement.

The global effectiveness indices for several meshes are given in Table 2. The strict upper bound is not achieved, which is attributed to the error in the solution of the local problem. If a more accurate estimate is needed, one may resort to a more complex procedure for the solution of the local problem.

As the error in the effectiveness index is considerable, we have repeated the calculation of the error estimate on the 20×11 CV mesh, exactly solving the local problem for every CV. The revised effectiveness index equals 1.017 and the discrepancy in the solution of the local problem is located next to the boundary, confirming the hypothesis.

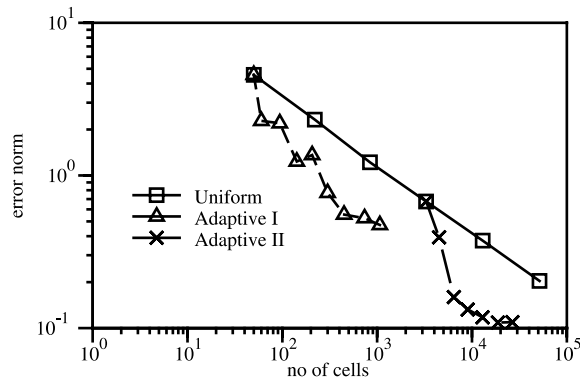


Fig. 8. Line source in cross flow: error scaling.

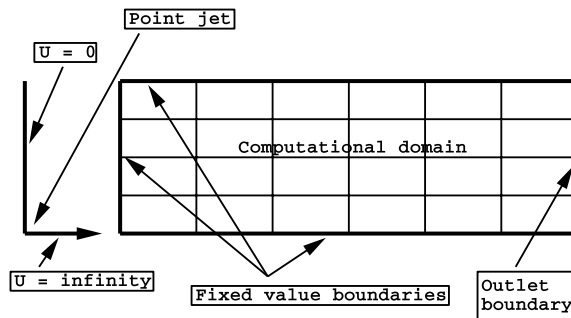


Fig. 9. Line jet: test setup.

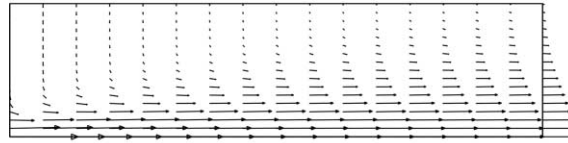
Fig. 11 shows the scaling of the estimated error with uniform mesh refinement for the meshes up to 51 520 CVs. It can again be seen that, once the boundary conditions are adequately resolved, the error estimate mirrors the second-order accuracy of the discretisation method.

5.4. Laminar flow over a 2-D hill

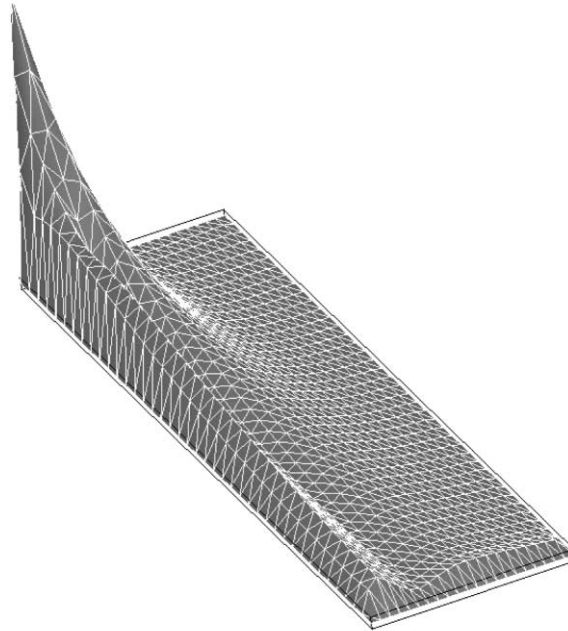
The final test case in this study represents a realistic fluid flow situation. It consists of a fully developed laminar duct flow hitting a hill-shaped obstacle of the height H . The Re number, based on the centreline velocity and the hill height is 60. The computational domain starts $3.6 H$ upstream of the hill summit and extends for $15 H$ downstream. The profile of the hill is given in Table 3.

The problem will be solved on a series of meshes created using transfinite mapping with slight grading towards the wall, ranging from 518 to 137 344 CVs. One of the meshes is shown in Fig. 12; the resulting velocity field can be seen in Fig. 13.

The estimated error norm distribution on the coarse mesh, Fig. 14, highlights two regions of high error. The first, at the front of the hill, is associated with the flow impingement and locally



(a) Exact solution



(b) Estimated error norm

Fig. 10. Line jet.

Table 2

Line jet: global error norm and effectiveness index

Mesh size	Global error norm	Global effectiveness index
10×5	0.393599	0.78347
20×11	0.319659	0.98313
40×21	0.017713	0.96943

high velocity gradients. The second error peak is associated with the combination of the velocity gradient in the shear region at the edge of the recirculation bubble and the change in mesh size (see Figs. 12 and 13).

The analytical solution for this test case is not available, which in effect prevents us from comparing the estimated and exact error norm. However, one can still examine the scaling of the estimated error with mesh refinement, presented in Fig. 15. For clarity, the estimated error has been normalised by the total dissipation in the system, obtained from the two finest meshes using Richardson extrapolation. As in previous cases, the error approaches the expected order of

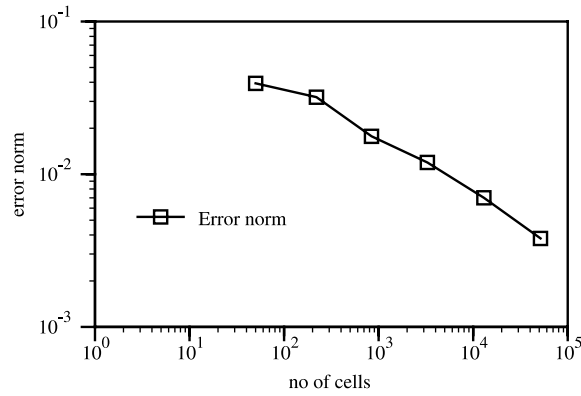


Fig. 11. Line jet: error scaling.

Table 3
The profile of the hill

x (mm)	0	9	14	20	30	40	54
y (mm)	28	27	24	19	11	4	0

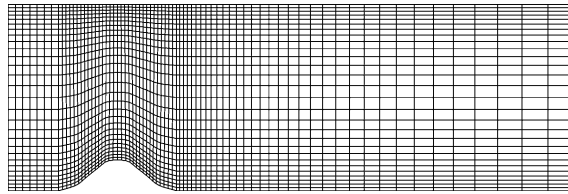


Fig. 12. 2-D hill: coarse mesh, 2044 CV.

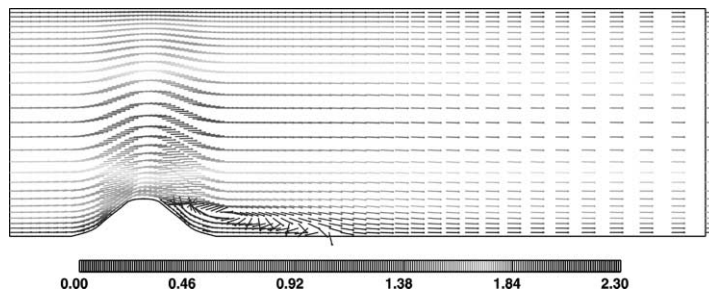


Fig. 13. 2-D hill: velocity field.

accuracy as the meshes become finer. The relative error has been reduced from 38% on the coarsest mesh to 0.3% on the finest.

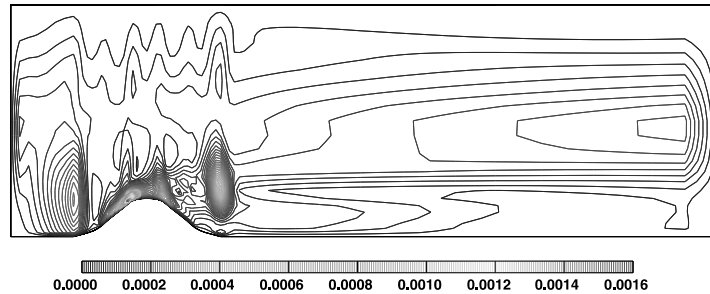


Fig. 14. 2-D hill: error distribution, 2044 CV.

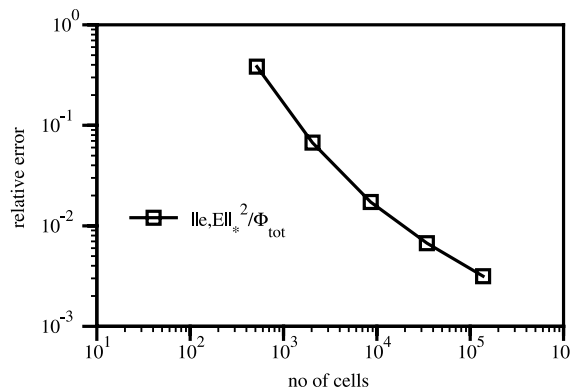


Fig. 15. 2-D hill: relative error in dissipation.

6. Summary

In this paper we have presented the extension of the EREE [1] to the FVM of discretisation. The EREE formulates the local residual error problem on a cell-by-cell basis, with the cell boundary conditions determined from the equilibrated error fluxes. In the FEM, the error estimate is reported to consistently produce the effectiveness indices close to unity.

The extension of the EREE to the FVM can be divided into several stages. First, it is necessary to reconstruct the cell residual as, unlike in the FEM, it does not arise naturally. The conservative properties of the FVM allow us to omit the error flux equilibration: it has been demonstrated that the balanced error fluxes are readily available from the solution itself. The EREE is completed with a simplified solution method for the local error problem consistent with the FV discretisation. Finally, the error estimate is tested on three test cases with analytical solutions and a realistic laminar flow situation. In all cases, the estimate shows good accuracy, similar to the one reported in the FEM and approaches the theoretical order of the discretisation when the mesh becomes fine enough.

The weakest point in the error estimate is the approximate solution method for the determinate local problem which causes the loss of the global error bound on coarse meshes. In terms of price/performance, the method presented here is considered adequate.

The objective of the work presented in this paper was to develop a simple and reliable a-posteriori error estimate whose computational cost is negligible compared to the cost of the solution itself. Future work will be concentrated on the performance of the error estimate on more complex mathematical models, specifically turbulent fluid flow. Ultimately, our goal is to assemble an error-driven solution-adaptive refinement procedure capable of automatically producing the solution to complex turbulent flow models of pre-determined accuracy at minimal cost.

References

- [1] Ainsworth M, Oden JT. A unified approach to a-posteriori error estimation using element residual methods. *Numerische Mathematik* 1993;65:23–50.
- [2] Ainsworth M, Oden JT. A procedure for a-posteriori error estimation for h - p finite element methods. *Comp Meth Appl Mech Engng* 1992;101:73–96.
- [3] Oden JT, Wu W, Ainsworth M. An a-posteriori error estimate for finite element approximations of the Navier–Stokes equations. *Comp Meth Appl Mech Engng* 1994;111:185–202.
- [4] Oden JT, Demkowicz L, Rachowicz W, Westermann TA. Toward a universal h - p adaptive finite element strategy. Part 2: a-posteriori error estimation. *Comp Meth Appl Mech Engng* 1989;77:113–80.
- [5] Ainsworth M, Oden JT. A posteriori error estimation in finite element analysis. New York: John Wiley and Sons; 2000.
- [6] Ainsworth M, Oden JT. A-posteriori error estimators for second-order elliptic systems: Part 2. An optimal order process for calculating self-equilibrating fluxes. *Comput Math Appl* 1993;26(9):75–87.
- [7] Ainsworth M. A-posteriori error estimators for second-order elliptic systems: Part 1. Theoretical foundations and a-posteriori error analysis. *Comput Math Appl* 1993;25(2):101–13.
- [8] Bank RE. A-posteriori error estimates. Adaptive local mesh refinement and multigrid iteration. In: *Lecture Notes in Mathematics Multigrid Methods II*. New York: Springer Verlag; 1986. p. 7–22.
- [9] Bank RE, Weiser A. Some a-posteriori error estimators for elliptic partial differential equations. *Math Comput* 1985;44:283–301.
- [10] Kelly DW. The self-equilibration of residuals and complementary a-posteriori error estimates in the finite element method. *Int J Numer Meth Engng* 1984;20:1491–506.
- [11] Oden JT, Wu W, Legat V. An h - p adaptive strategy for finite element approximations of the Navier–Stokes equations. *Int J Numer Meth Fluids* 1995;20:831–51.
- [12] Berger MJ, Olinger J. Adaptive mesh refinement for hyperbolic partial differential equations. *J Comp Phys* 1984;53:484–512.
- [13] Berger MJ, Collela P. Local adaptive mesh refinement for shock hydrodynamics. *J Comp Phys* 1989;82:64–84.
- [14] Berger MJ, Jameson A. An adaptive multigrid method for the Euler equations. *Lect Notes Phys* 1985;218:92–7.
- [15] Thompson MC, Ferziger JH. An adaptive multigrid technique for the incompressible Navier–Stokes equations. *J Comp Phys* 1989;82:94–121.
- [16] McGuiirk JJ, Taylor AMPK, Whitelaw JH. The assessment of numerical diffusion in the Upwind-Difference calculations of turbulent recirculating flows. In: Bradbury LJS, Durst F, Launder BE, Schmidt FW, Whitelaw JH, editors. *Selected papers from the Third International Symposium on Turbulent Shear Flows, Turbulent Shear Flows*, vol. 3. The University of California, Davis, September 9–11 1981. p. 206–24.
- [17] McGuiirk JJ, Rodi W. A depth-averaged mathematical model for the near field of side discharges into open channel flow. *J Fluid Mech* 1978;86:761.
- [18] Haworth DC, El Tahry SH, Huebler MS. A global approach to error estimation and physical diagnostics in multidimensional fluid dynamics. *Int J Numer Meth Fluids* 1993;17(1):75–97.
- [19] Muzafferija S, Gosman D. Finite-volume CFD procedure and adaptive error control strategy for grids of arbitrary topology. *J Comp Phys* 1997;138(2):766–87.
- [20] Jasak H, Gosman AD. Automatic resolution control for the finite volume method. Part 1: A-posteriori error estimates. *Numer Heat Transfer, Part B* 2000;38(3):237–56.

- [21] Jasak H. Error analysis and estimation in the finite volume method with applications to fluid flows, PhD thesis. Imperial College, University of London, 1996.
- [22] Jasak H, Gosman AD. Residual error estimate for the finite volume method. *Int J Numer Meth Fluids* 2001;39: 1–19.
- [23] Theodoropoulos T. Prediction of three-dimensional engine flow on unstructured meshes, PhD thesis. Imperial College, University of London, 1990.
- [24] Ferziger JH, Perić M. *Computational methods for fluid dynamics*. Berlin-New York: Springer Verlag; 1995.
- [25] Gosman AD. Developments in industrial computational fluid dynamics. *Trans I Chem E* 1998;76(A):153–61.
- [26] Girault V, Raviart P-A. *Finite element methods for Navier–Stokes equations*. In: Springer Series in Computational Mathematics, vol. 5. New York: Springer-Verlag; 1986.
- [27] Temam R. *Navier–Stokes equations: Theory and numerical analysis*. 2nd ed. Amsterdam: North-Holland; 1985.
- [28] Ainsworth M, Oden JT. A-posteriori error estimates for Stokes’ and Oseen’s equations. *SIAM J Numer Anal* 1997;34(1):228–45.
- [29] Hinze JO. *Turbulence*. New York: McGraw-Hill; 1975.
- [30] Jasak H, Gosman AD. Automatic resolution control for the finite volume method. Part 2: Adaptive mesh refinement. *Numer Heat Transfer, Part B* 2000;38(3):257–72.
- [31] Panton RL. *Incompressible flow*. New York: John Wiley and Sons; 1984.